Geochronology, 8, 785–798, 2026
https://doi.org/10.5194/gchron-8-785-2026
© Author(s) 2026. This work is distributed under
the Creative Commons Attribution 4.0 License.

Improving the estimation of high natural luminescence doses using OTOR solutions for SAR-derived data

Barbara Mauz[1], **Sebastian Kreutzer**[2,3], **and John Lawless**[4]

[1]Department of Environment and Biodiversity, University of Salzburg, 5020 Salzburg, Austria
[2]LIAG Institute for Applied Geophysics, 30629 Hannover, Germany
[3]Institute of Geography, Heidelberg University, 69120 Heidelberg, Germany
[4]Redwood Scientific, Pacifica, CA, USA

Correspondence: Barbara Mauz (barbara.mauz@plus.ac.at)

Received: 22 July 2026 – Discussion started: 25 August 2026
Revised: 29 October 2026 – Accepted: 12 November 2026 – Published: 24 November 2026

Abstract. In luminescence dating, dose-response curve fitting is critical to obtain dose estimates that are equivalent to the natural dose. For high natural doses several fitting functions are in use, but dose underestimation remains a common result. To address this, we analyse two functions directly derived from the one trap one recombination centre (OTOR) model alongside the single-saturating exponential function (SSE), typically used for data generated by a single-aliquot regenerative dose protocol (SAR) and, we test fit parameters using a set of natural samples.

Combining theory with empirical evidence we show, in agreement with earlier studies, that OTOR and SSE functions are the same in terms of their parameterisations, with OTOR allowing for one extra degree of freedom represented by the parameter $R = A_n/A_m$. By allowing R to vary, OTOR produces dose-response curves with high statistical significance. SSE produces dose-response curves that show "early" bending towards a dose plateau because, as theory reveals, it assumes that A_n/A_m is fixed at unity. Empirically however, R values are ~ 0.26 (quartz) and ~ 0.40 (K-rich feldspars) confirming the observed sublinear response to increasing doses, which is stronger with quartz than with feldspars. For both dosimeters extracted from our natural samples, the OTOR-derived characteristic saturation dose is 30 %–50 % higher than the D_0 value obtained from the SSE function. We provide full explanation why the D_0 parameter is always underestimated for quartz and feldspars. Overall, the OTOR solutions are beneficial, not least due to the physical meaning of the fit parameters derived from the simplest possible model.

1 Introduction

While highly desired, it remains a challenge for luminescence dating to determine high doses, hence high ages (e.g., > 300 ka). When employing the single aliquot regenerative (SAR) dose measurement protocol, the challenge is to project a natural dose close to saturation to a dose-response curve generated with high laboratory doses. The single-saturating exponential (SSE) function mostly delivers poor fits to this type of dose responses and equivalent doses obtained from such fits are likely inaccurate (Timar-Gabor and Wintle, 2013). Other functions are employed, mostly the single saturating exponential plus linear function (e.g. Tribolo et al., 2022) or the double exponential function (e.g. Timar-Gabor et al., 2015). These functions include constants that have no direct physical meaning and this, in turn, is inconsistent with the luminescence measurement parameters (e.g. detection wavelength) by which the signal from a dosimeter's specific trap-hole pair is targeted out of a broad light spectrum. It is therefore beneficial to employ a physically based model that allows to interpret observations obtained from responses to high laboratory doses.

Dose-response curve fitting is critical to obtaining reliable equivalent doses (e.g. Grün and Rhodes, 1992) and has been discussed accordingly in earlier studies (e.g. Bulur and Özer, 1992; Lyons et al., 1992). Since the SAR measurement protocol (Murray and Wintle, 2003) was introduced, Bailey (2001) and subsequent studies (e.g. Singarayer and Bailey, 2004) showed that the SSE is the appropriate fit function for individual quartz OSL components. From this Win-

tle and Murray (2006) concluded that for high natural doses the limit for determining reliably the equivalent dose (D_e) is at ca 86 % of the saturated value, hence the rule of thumb of $D_e < 2D_0$, where D_0 is 63 % of the saturated value. Although not explicitly stated, this recommendation implied the accurate determination of the saturation intensity I_{sat} and, as a consequence, highly variable D_0 values are reported (e.g. Thomsen et al., 2016).

Alongside the difficulty to determine I_{sat} when using the SSE, underestimation of D_e was reported frequently (e.g. Murray et al., 2007; Moska et al., 2012). Such underestimations are typically evident by a suppressed laboratory-generated DRC relative to the natural dose response and explained by the competition for free electrons from the R centre that is low during natural and high during laboratory irradiation (Bailey, 2004). The natural build-up of dose would therefore be different to laboratory-induced build-up, resulting in a different shape of the dose-response curve (Chapot et al., 2012; Timar-Gabor and Wintle, 2013; Peng et al., 2022). Although empirically often not confirmed (e.g. Chapot et al., 2012), the value of I_{sat} should be the same for natural and laboratory-induced DRCs unless loss of trapped electrons occurred during burial (Peng et al., 2022). Chapot et al. (2012) and Timar-Gabor and Wintle (2013) agree that the growth of the natural dose can be described by the SSE and that the laboratory-induced DRC is best described using the sum of two exponential functions. This is confirmed by Peng et al. (2022) who simulated quartz DRCs using the Bailey (2001) kinetic model with slightly modified parameters. The results from the simulation suggest competition for free electrons, either in the deep electron trap of the natural sample or in the recombination centres of the irradiated sample (Peng et al., 2022). This well-known competition between trap and recombination centre during irradiation (Bailey, 2004) has prompted different statements: the competition for electrons in the deep trap is dose-dependent which should explain the second saturating exponential component in the DRC (Peng et al., 2022) or, the competition effects result in non-linear dose dependence of the luminescence signal, even at relatively low laboratory doses depending on the trapping probability of electrons in traps, and the trapping probability of holes in centres, as well as on the recombination probability of free electrons with trapped holes in the centres (Lawless et al., 2009). For the latter case, D_0 may not be independent of the range of regeneration doses in a SAR measurement protocol (Murray et al., 2021) and the resulting D_e is then dependent on the model of luminescence response to dose.

Here we explore the analytical expression, *Lambert W*, developed by Pagonis et al. (2020) and the OTORX function (Lawless and Timar-Gabor, 2024). Both functions are an exact solution of the OTOR (one trap and one recombination centre) model, with OTOTX allowing for an additional, deeper, trap to take part in the irradiation process. The well-studied OTOR model (e.g., Kitis et al., 2019, 2025) suggests that the shape of the dose-response curve (DRC) depends on A_n/A_m which is the ratio of the recombination to retrapping rate constants. If $A_n/A_m \sim 1$, both the OTOR and the SSE functions agree and the DRC shape is the same (Pagonis et al., 2020). For A_n/A_m, we establish values empirically for quartz (see also Kitis et al., 2022) and for feldspar dosimeters, and we use the OTOR model to understand the significance of the SSE-derived D_0 parameter and to find the reason for the often reported D_e underestimation.

2 Material and methods

2.1 Samples and luminescence measurements

The samples used in this study are fine- and coarse-grained feldspar and quartz samples originating from coastal or aeolian environments to ensure sufficient bleaching at time of deposition (Table 1).

The L_x/T_x data, required to undertake the analysis, were obtained from published datasets (see Table 1 for references) or from samples currently analysed in our laboratory (see Sbg-samples in Table 1). The latter were measured using the $pIRIR_{225}$ protocol (Thomsen et al., 2008) with integration intervals of 0.06 s for the signal and last 60 s for the background to be subtracted. The detection window used was 410Δ10 nm (BG39 + HC414/46) in a *Lexyg Smart* reader equipped with a UV-VIS photomultiplier tube (300–650 nm) and IR light stimulation (850Δ5 nm) delivering 100 mW cm^{-2} at sample position. The dose points selected followed doubling of the initial dose step (i.e. 1, 2, 4, 8, ...; e.g. Grün and Rhodes, 1992) with the maximum laboratory dose being around 5000 Gyr. It is assumed that the sensitivity change occurring during the measurement of the natural OSL is negligible and that all sensitivity change occurring during the measurement of laboratory-dose induced OSL is correctly monitored by the test dose OSL/IRSL.

2.2 Generating dose-response curves

The experimental data were fitted using the three fit functions SSE, OTOR, and OTORX, each delivering the relevant fit parameters. These are $R = A_n/A_m$, D_{63} and c for OTOR(X) and D_0 for SSE (for details see next paragraph). To avoid confusion, the characteristic saturation dose derived from the OTOR functions is called D_{63}, the one derived from SSE is called D_0, both representing 63 % of the saturation dose I_{sat}.

Two codes, one written in Python and the other one written in R (R Core Team, 2026), were employed. The Python code 3.13.5 (main, 5 May 2026, GCC 14.2.0) uses the SciPy package version 1.15.3. The R implemented used the package "Luminescence" (Kreutzer et al., 2026) and the function `Luminescence::fit_DoseResponseCurve(..., fit.method = c("EXP", "OTOR", "OTORX")`. Both codes use to some extent the Fortran MINPACK library (Moré et al., 1980).

Table 1. Characteristics and origin of samples used in this study.

Sample	Dosi-meter	Grain Size (µm)	Sample origin	Sample reference
Sbg 426	Feldspar	4–11	Aeolian dust	This study
Sbg 452	Feldspar	4–11	Aeolian dust	This study
Sbg 453	Feldspar	180–300	Desert sand sheet	This study
Sbg 457	Feldspar	180–300	Desert sand sheet	This study
BAT1.19A	Feldspar	4–11	Aeolian dust	Avram et al. (2020)
XY575	Feldspar	4–11	Aeolian dust	Avram et al. (2022)
XY575	Feldspar	4–11	Aeolian dust	Avram et al. (2022)
Love7	Feldspar	4–11	Aeolian dust	Avram et al. (2025)
Love6	Feldspar	4–11	Aeolian dust	Avram et al. (2025)
Stayky	Feldspar	4–11	Aeolian dust	Veres et al. (2018)
CAC_2.1	Quartz	4–11; 63–90	Aeolian dust	Timar-Gabor et al. (2017)
CST_{inf}	Quartz	4–11; 63–90	Aeolian dust	Timar-Gabor et al. (2012)
M#6#	Quartz	4–11; 63–90	carbonate aeolianite	Timar-Gabor et al. (2017)
BT844	Quartz	4–11	Aeolian dust	Meszner et al. (2013)
BT755	Quartz	4–11	Aeolian dust	Fuchs et al. (2013), Dataset: Fuchs et al. (2023)
BT754	Quartz	4–11	Aeolian dust	Fuchs et al. (2013), Dataset: Fuchs et al. (2023)
BT753	Quartz	4–11	Aeolian dust	Fuchs et al. (2013), Dataset: Fuchs et al. (2023)
XF153_A	Quartz	4–11	Aeolian dust	Timar-Gabor et al. (2017)
XY575	Quartz	4–11	Aeolian dust	Avram et al. (2022)
Stayky	Quartz	4–11; 63–90; 180–250	Aeolian sand	Veres et al. (2018)
Love5	Quartz	63–90	Aeolian sand	Avram et al. (2025)
Love6	Quartz	63–90	Aeolian sand	Avram et al. (2025)
BAT1.19_A	Quartz	4–11; 63–90	Aeolian sand	Avram et al. (2020)
MV10	Quartz	4–11	Aeolian dust	Timar-Gabor et al. (2012)
MST19	Quartz	4–11; 63–90	Aeolian dust	Timar-Gabor et al. (2012)

Both codes use standard approaches (non-linear least-squares and Levenberg-Marquardt algorithm as discussed in Hayes et al., 1998) with the uncertainty being determined through weighting by the inverse variance. This includes forcing the fit to go through the zero point (L_0/T_0 from a SAR protocol). This value varies according to the sample's specific response to laboratory dosing and according to the selection of the integration time intervals (Cunningham and Wallinga, 2010).

3 Analysis of the dose-response curve functions

The dose response of dosimeters used in luminescence dating is the result of the trap-filling process during irradiation followed by thermal or optical stimulation. The resulting luminescence signal is proportional to the concentration of filled traps modified by the competition effects between traps and recombination centres during thermal or optical stimulation (Pagonis et al., 2020). The simplest model that describes the irradiation process, is the one trap one recombination centre (OTOR) model (McKeever and Chen, 1997). This fundamental model is useful for SAR-derived data because it can be described by a physics-based equation for the dose response, $n(D)/N$:

$$\frac{n(D)}{N} = 1 + \frac{\mathcal{W}\left\{(R-1)\exp\left(R-1-\frac{D}{D_c}\right)\right\}}{1-R} \quad (1)$$

where $\mathcal{W}$ is the Lambert function, $R = A_n/A_m$, D is the irradiation dose and D_c is a characteristic dose. For details about the derivation of this equation see Lawless et al. (2009) and Pagonis et al. (2020). Within the OTOR model, R is understood as the ratio of the trapping coefficient of the electron trap to the recombination coefficient of the recombination centre. If measured in units of electron-hole pairs created per volume, the characteristic dose $D_c = N/R$ where N is the total concentration of the electron trap. If $R = 1$, then D_c is the total dose, $D + D_i$ at which the OSL intensity is 63 % of saturation, just like the SSE formula. If $R = 0.2$, as might be typical for quartz (Lawless and Timar-Gabor, 2024), then D_c is the total dose, $D + D_i$, at which the OSL intensity is 81 % of saturation. In other words, the normalised OSL intensity (I/I_{sat}) is a function of R when the total dose is D_c (Fig. 1). On a DRC, small R values correspond to strong sublinearity.

An important feature of the OTOR formula is that its DRCs are not self-similar, i.e. plots of I/I_{sat} versus $(D + D_i)/D_{63\,\%}$ do not overlap, unless they have the same R. In contrast, the same normalised plots produced through the SSE function overlap, because in the SSE formula $R = 1$,

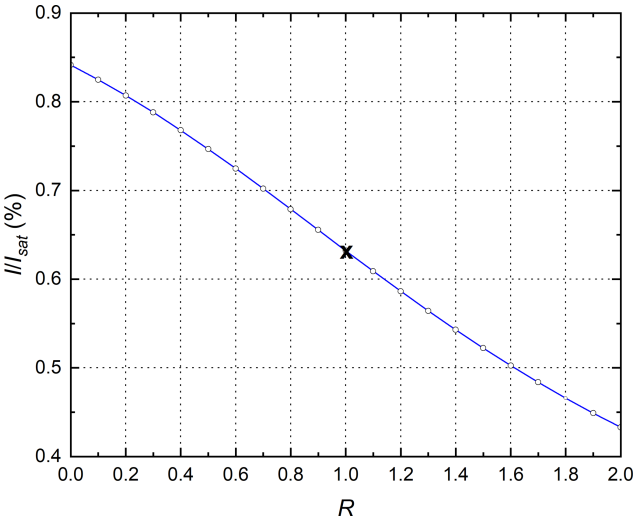

Figure 1. The OSL intensity relative to the normalised saturation intensity as a function of R when total dose is D_c as derived from Eq. (1). For $R = 1 I/I_{sat} = 0.63\,\%$.

hence the same for all plots. Thus, the OTOR-derived formula provides the flexibility to fit a wide variety of DRC.

An alternative formulation of the OTOR model, called OTORX, is given by Lawless and Timar-Gabor (2024) where equations are modified to use D_{63} as a fitting parameter:

$$I = I_{sat}\left[1 + \frac{1}{Q}\mathcal{W}(-(1-R) \cdot \exp\left[-\left(1 - \frac{e-1}{e}(1-R)\right)\ \frac{D+D_i}{D_{63}} - (1-R)\right]\right)\right] \quad (2)$$

where Q is

$$Q = \frac{A_m - A_n}{A_m}\frac{N}{N+N_D}$$

and D_{63} is the dose at which $I = 0.63 I_{sat}$; all other factors are defined as in Eq. (1).

For SAR-derived data, Eq. (2) is normalised in the same way as it is done for SAR data:

$$\frac{L_x}{T_x} = c\frac{1 + \frac{1}{Q}\mathcal{W}\left(-(1-R)\exp\left[-\left(1-\frac{e-1}{e}(1-R)\right)\ \frac{D+D_i}{D_{63\,\%}} - (1-R)\right]\right)}{1 + \frac{1}{Q}\mathcal{W}\left(-(1-R)\exp\left[-\left(1-\frac{e-1}{e}(1-R)\right)\ \frac{D_T+D_i}{D_{63\,\%}} - (1-R)\right]\right)} \quad (3)$$

where D_T is the test dose and all other factors are defined as in Eqs. (1) and (2).

In Eq. (3) I_{sat} no longer appears due to the normalisation, and is replaced by c to monitor the correction for sensitivity changes. If the sensitivity changes are corrected perfectly, c is 1. However, for most materials c is only within 20 % of one.

Thus, Eq. (3) involves 4 parameters:

- D_{63} (%) is the dose at which the luminescence intensity reaches 63 % of the saturation dose, $I = 0.63 I_{sat}$.
- R is the ratio of the trapping coefficient of the electron trap to the recombination coefficient of the recombination centre: $R = A_n/A_m$ called retrapping ratio.
- c is the correction for a systematic change in sensitivity occurring during readouts of the regenerated dose OSL and subsequent test dose OSL. If c differs strongly from 1, then protocol and/or dosimeter are perhaps not appropriate.
- D_i reflects the fact that OSL signal is measured even with zero applied dose, typically observed as recuperation signal.

Next, we examine the ability of the OTOR and SSE fit functions to determine the physical parameters R, D_{63} and D_0, when the data to be fitted cover the low dose range, i.e., only the lower segment of a DRC composed of slope and curvature is covered by the data. By generating relevant mathematical formulation (see Eqs. A2 to A11 in Appendix), we find that error margins for D_{63} are large. To assess the error margins, the D_{63} value computed at value R ($D_{63actual}$) is compared to the D_0 value for $R = 1$ (Fig. 2) using this equation:

$$\frac{D_{63actual}}{D_0} = \frac{1 + (e-1)R}{eR^2} \quad (4)$$

The plot in Fig. 2 shows that the ratio $D_{63actual}/D_0$ increases in a non-linear manner with decreasing R values implying that for DRCs restricted to the low segment, the SSE model underestimates the characteristic saturation dose D_0 when $R < 1$. When $R < 0.5$, the underestimation is significant.

Next, we test the control of the parameter R on the shape of the DRC by fitting the dose normalised to the characteristic saturation dose against the luminescence intensity normalised to the saturation intensity for various values of R using the OTOR function. In theory, the DRCs should not overlap and should intersect at $I/I_{sat} = 0.63$ and $(D+D_i)/D_{63} = 1$. Using selected samples analysed in this study, we plot I/I_{sat} vs. D/D_{63} (Fig. 3): the lower segment of the curves appears to overlap due to generally small L_0/T_0 values and the intersection point (see cross in Fig. 3) is a cluster of data points ranging from 0.6 to 0.7 at $D/D_{63} = 1$ due to measurement uncertainty. Thus, the DRC shape is quasi-identical for luminescence intensities up to D_{63} (or slightly below D_{63}) as long as the curves' zero-points are close to zero. The DRC shape varies beyond D_{63} according to the sample's R value. This demonstrates that the fit parameters R and D_{63} are key to accurately determine an equivalent dose from a sublinear DRC.

In summary, our mathematical analysis reiterates what has been shown already by Pagonis et al. (2020), by Lawless

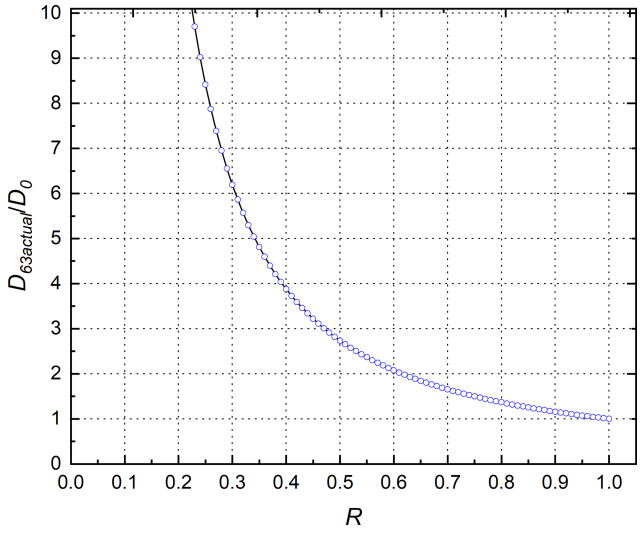

Figure 2. The ratio D_{63} actual to D_0 plotted against R values ranging from 0.1 to 1, using Eq. (4) (see Appendix A for details). For $R = 1$ the ratio is 1.

and Timar-Gabor (2024) and by Kitis et al. (2025): (i) direct solutions of the OTOR model exist and these solutions are suitable to fit data derived from a SAR-based measurement protocol, (ii) the solutions provide fit parameters that are physically meaningful, (iii) the SSE function is a solution of OTOR for $R = 1$. Our mathematical analysis expand this knowledge by specifically analysing long versus short DRCs where a long DRC includes enough data points at high dose that the saturation intensity can be determined. Quantitatively speaking, a long DRC includes multiple dose points at $D/D_{63} > 10$ (see Fig. 3A). When fitting a short DRC, the SSE function underestimates D_0 of those dosimeters for which R is actually smaller than 1. For the same short DRC, the OTOR model yields accurate D_{63} values with large error margins.

4 Results from experiments

Experiments were conducted to obtain fit parameters from SSE and OTOR(X) fit functions for a set of L_x/T_x data (for samples see Table 1), to obtain R values, examine fit parameters (D_0, D_{63} and R) and to assess fit quality using the chi-squared test. The results are listed in Table 2.

For one quartz and one feldspar sample c deviates strongly from the expected value of 1. The values of D_0, D_{63} and R obtained from these samples are therefore questionable and were excluded from further examination. R values obtained from the remaining samples are on average 0.26 (±27 %) for quartz and 0.41 (±20 %) for feldspar. The ratio of D_0 (derived from SSE) and D_{63} (derived from OTOR) is on average 0.54 for quartz and 0.65 for feldspar, i.e. D_0 is around 46 % (quartz) and 35 % (feldspar) lower than D_{63} (Table 2; Fig. 4).

The quality of the SSE and OTOR(X) fits as shown in Fig. 5 is assessed using the chi-squared test with smaller χ^2 values indicating higher statistical significance. The ratio $\chi^2_{SSE}/\chi^2_{OTOR}$ is greater than 1 when the OTOR fit is more significant and hence, the poorer the SSE fit, the higher the ratio. Figure 6 shows that most feldspar ratios and all quartz ratios are above 1, some by a factor of 10 or more (for data see Table 2).

5 Discussion

In the empirical part of this study, the number of samples per dosimeter as well as the number of aliquots measured per sample, is small. The small number precludes a quantitative assessment of the experimental data, which is why uncertainties of individual parameter values are not meaningful and, hence, not listed in Table 2 and not shown in relevant figures. However, the empirical data compared with the mathematical analysis of the OTOR model (Sect. 3 and Appendix A) allow us to infer usefulness and limitation of the OTOR fit functions for determining high natural doses using SAR protocols. This enables us to discuss the role of I_{sat} and A_n/A_m and thereby understand the D_e underestimation caused by the SSE.

5.1 DRC shape and quality of fit

The usefulness of the OTOR functions lies in the physical meaning of its parameters, where c allows to infer how suitable the measurement protocol and/or the sample is, R is a measure of the shape of the DRC and D_{63} is the characteristic saturation dose as is the parameter D_0 of the SSE function.

The shape of the DRC is a function of experimental uncertainties, and the goodness of fit. Given the importance of the DRC shape for determining D_e, R provides a quality check for the D_e determined if its value can be predicted. Our R values for quartz (∼ 0.26) are close to the ones published so far (e.g. Kitis et al., 2022; Lawless and Timar-Gabor, 2024) and slightly lower than those obtained from feldspars (∼ 0.41). However, a statistically significant difference between the two dosimeters does not appear in our data: both dosimeters can show any R value between 0.10 and 0.55 (Fig. 3) with quartz tending to lower R values, hence stronger sublinearity, than feldspar. Some R values (Table 2) suggest dependence on measurement protocol where the $pIRIR_{290}$ protocol tends to deliver higher R values than the $pIRIR_{225}$ protocol. Similarly, larger grain sizes seem to deliver higher R values than smaller grain sizes (Fig. 7). However, with the statistical noise not being quantifiable in our study, these trends remain untested.

The goodness of fit is quantified by the reduced chi-square (RCS) with RCS < 5 being regarded as indicating a satisfactory fit (Peng and Li, 2017). We examine the chi-squared ratio ($\chi^2_{SSE}/\chi^2_{OTOR}$; Table 2) as statistical significance of the SSE and OTOR fits and note that the OTOR functions im-

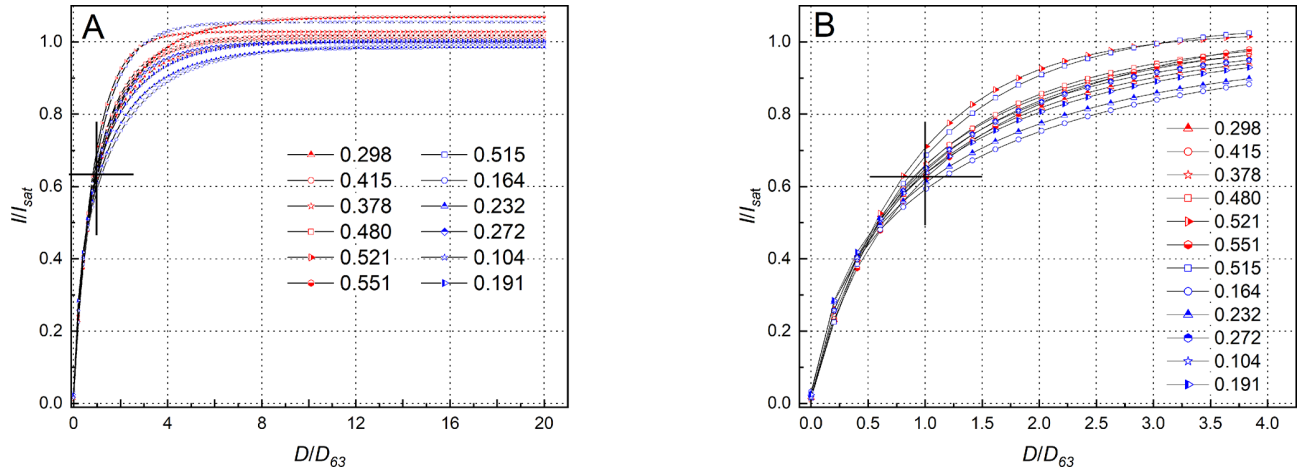

Figure 3. The luminescence intensity (I) normalised by the intensity at saturation (I_{sat}) plotted against the laboratory dose (D) normalised by D_{63} for various values of R derived from quartz (blue) and feldspar (red) data. **(A)** all data; **(B)** lower segment of the curves shown in **(A)**. For values of R and D_{63} see Table 2.

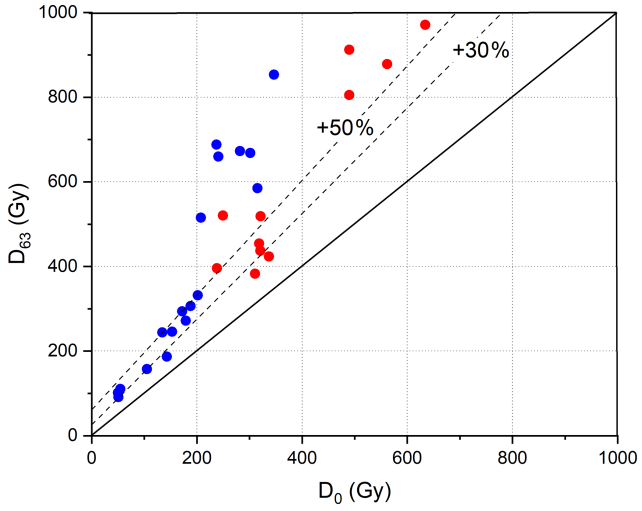

Figure 4. The D_{63} values plotted against the D_0 values for quartz (blue) and feldspar (red) samples. Lines indicate the 1 : 1 relationship and the +30 % and +50 % deviation.

proves the fit quality for almost all samples regardless the dosimeter (Fig. 6). Thus, the fit improvement compensates for the one extra degree of freedom that OTOR has compared to SSE. However, the improved fit quality is not independent of R: where R is outside the predicted value range, the OTOR fit quality is reduced (Fig. 6).

With the consistencies apparent so far, we can say that R is always smaller than 1, most probably smaller than 0.5. The impact of $R < 0.5$ is shown by the normalised D_{63} (Fig. 2) and by the normalised fit curves (Fig. 3): both the D_0 value and the shape of the DRC imply D_e underestimation where the inaccuracy of the D_e estimate becomes significant when projecting a natural dose onto the upper DRC segment, hence above $\sim D_0$. The empirical data confirm this by D_0 being 30 %–50 % lower than D_{63} (Fig. 4). Unrealistic R values (e.g. 0.01…, 2.0…) indicate an irradiation process that cannot be described by the OTOR model. Conversely, natural doses projected onto a SSE-fitted DRC are reliable for the lower segment because this DRC segment is negligibly affected by the fact that R is actually smaller than 1 (Fig. 3) as long as the recuperated signal is small. With Eqs. (4) and (A2)–(A12) in mind, it is clear that this statement is valid for long DRCs only. If the DRC is short, D_0 is underestimated (Fig. 2) and the separation between lower and upper DRC segment is difficult to quantify. This is evident from studies on standardised growth curves (e.g. Hu et al., 2019) demonstrating remarkably the variability of quartz DRCs, apparently caused by variable D_0 values of individual grains. Here, the OTOR functions are indeed useful, because they allow to double check fit parameters (e.g. D_0, I_{sat}) required to establish standardised growth curves.

5.2 The role of the saturation intensity I_{sat}

The value of I_{sat} is needed to accurately determine D_{63} and the value of D_{63} is required to assess the reliability of the saturation dose as shown by Eq. (3) and Figs. 2 and 3. Determining I_{sat} is a non-trivial task: quartz DRCs tend to show a non-monotonic shape (e.g. Duller, 2012) which was explained with "dose quenching", i.e. loss of recombination centres (Huntley et al., 1996) or with competition taking place during irradiation or during read-out (Lawless et al., 2005). The DRC of feldspar seem to reach a dose plateau (Fig. 5), but the corresponding dose is likely underestimated due to signal instability (Kars et al., 2008; King et al., 2018). Moreover, the study of Peng et al. (2022) suggests that there is a dose-dependent change of signal growth due to dose-dependent change in competition for free electrons in the deep trap.

Table 2. Fit parameter values for D_0, D_{63}, R, c, and fit quality parameter ratio of the reduced chi-square $\chi^2_{SSE}/\chi^2_{OTOR}$ obtained from the average of n measured aliquots using SSE, OTOR and OTORX fit functions where applicable. β_{max} is the maximum laboratory dose administered; * excluded from further examination.

Sample	Protocol	n	β_{max} (Gyr)	D_0(SSE)	D_{63}	R	c	$\chi^2_{SSE}/\chi^2_{OTOR}$
Feldspar ($n = 13$)								
Sbg 426	$pIRIR_{225}$	3	4812	303	422	0.36	1.024	10.54
Sbg 452	$pIRIR_{225}$	3	2355	318	454	0.424	0.936	12.25
Sbg 453	$pIRIR_{225}$	3	2816	337	424	0.521	0.951	1.024
Sbg 457	$pIRIR_{225}$	3	2816	311	383	0.551	0.936	1.052
BAT_1.19A	$pIRIR_{290}$	3	5000	238	396	0.371	1.106	20.3
BAT_1.19A	$pIRIR_{225}$	3	5000	321	519	0.301	1.062	198.9
XY575	$pIRIR_{290}$	3	5000	249	521	0.315	1.015	152.4
XY575*	$pIRIR_{225}$	3	5000	231	3213	0.061	0.914	134.9
Love7	$pIRIR_{290}$	3	5000	562	878	0.378	0.972	172.1
Love7	$pIRIR_{225}$	3	5000	634	971	0.364	0.976	69.4
Love6	$pIRIR_{290}$	3	5000	490	805	0.497	0.956	100.3
Love6	$pIRIR_{225}$	3	5000	490	912	0.415	0.969	38.7
Stayky*	$pIRIR_{290}$	1	10 000	283	1398	0.022	1.38	0.144
Quartz ($n = 21$)								
BT844	SAR-OSL	3	1200	179	272	0.329	1.185	25.90
BT755	SAR-OSL	2	1200	179	272	0.328	1.202	38.1
BT754	SAR-OSL	2	1200	188	307	0.302	1.269	51.6
BT753	SAR-OSL	2	1200	202	332	0.305	1.215	31.3
$XY575_{4-11*}$	SAR-OSL	3	5000	241	660	0.191	0.376	71.3
$Stayky_{4-11}$	SAR-OSL	3	10 000	237	688	0.223	1.046	39.6
$Stayky_{180-250}$	SAR-OSL	4	5000	50.8	91.2	0.256	1.180	107.5
$Stayky_{63-90}$	SAR-OSL	3	5000	50.1	102	0.222	1.182	230.4
Love6	SAR-OSL	3	5000	153	246	0.232	1.139	4.6
Love5	SAR-OSL	3	5000	134	244	0.216	1.216	19.8
$BAT1.19A_{63-90}$	SAR-OSL	3	5000	54	111	0.323	1.144	171.3
CST_inf_{4-11}	SAR-OSL	2	9984	302	668	0.184	1.056	23.6
CST_inf_{63-90}	SAR-OSL	2	5245	143	187	0.376	1.082	15.0
$CAC_2.1_{4-11}$	SAR-OSL	1	5000	285	673	0.173	1.011	11.2
$CAC_2.1_{63-90}$	SAR-OSL	1	5000	99	184	0.153	1.137	11.9
$M\#6\#_{4-11}$	SAR-OSL	3	6000	315	585	0.137	1.191	4.95
$M\#6\#_{63-90}$	SAR-OSL	3	2060	105	158	0.343	1.251	737.6
$MST19_{4-11}$	SAR-OSL	1	5114	346	853	0.146	1.104	45.0
$MST19_{63-90}$	SAR-OSL	1	5002	172	294	0.167	1.101	20.5
MV10	SAR-OSL	1		314	808	0.110	1.091	52.1
$XF_153_A_{4-11}$	SAR-OSL	2	5000	208	515	0.184	1.087	32.2

As dose grow, the efficiency of the trap in capturing free electrons diminishes while the recombination rate becomes stronger (Lawless et al., 2009), hence the sublinear dose response with $R < 1$. Thus, long DRCs are required to reliably determine the OTOR fit parameters. These long DRCs may or may not include I_{sat} but must be, at least, close to I_{sat}.

5.3 Underestimation of high natural doses

The data generated in this study suggest that D_es obtained from the SSE fit and determined in the dose range 100–1000 Gyr are ca. 10 %–30 % smaller than those obtained from the OTOR fit (Fig. 8). Our data echo the many age underestimations reported for quartz (e.g. Lowick and Preusser, 2011; Timar et al., 2010; Timar-Gabor and Wintle, 2013). Quantifying the underestimation for feldspars requires fading correction using the OTOR function (e.g. Guralnik and King, 2026).

Approaches that circumvent the problem were proposed: selecting "supergrains" out of the grain population sampled (Yoshida et al., 2000), i.e. grains exhibiting D_0 values that are close to the expected D_e value (e.g. Arnold et al., 2016) or, the weighted mean natural dose (L_n/T_n) of all measured grains is projected onto a standardised growth curve (Li et al., 2016). Both approaches rely on correct estimation of the

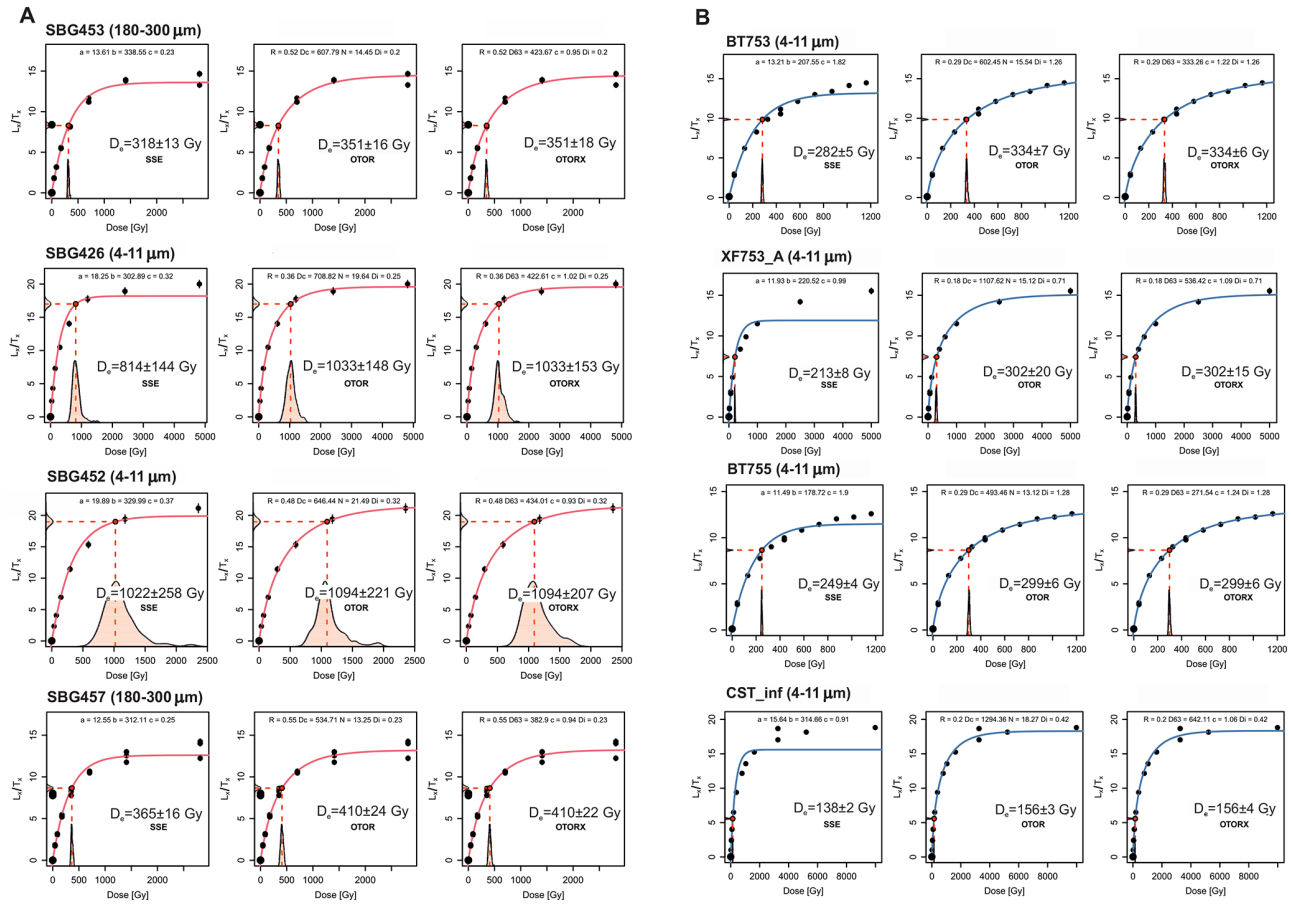

Figure 5. Interpolation of L_n/T_n onto DRCs generated using SSE, OTOR and OTORX functions; **(A)** feldspar samples; **(B)** quartz samples, both including grain size. Each panel shows the D_e value and the fit parameter values.

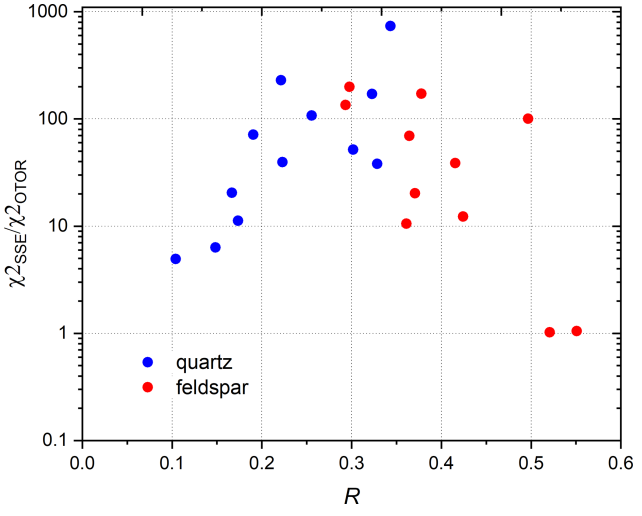

Figure 6. The statistical significance of the SSE and OTOR fits for feldspar and quartz samples plotted against the OTOR fit parameter R. Note log scale of y axis.

D_0 value. However, this value is underestimated for long DRCs (Fig. 4) and, probably even more pronounced, for short DRCs (Fig. 2).

The often used alternative to the SSE is the double exponential (DSE) function. In fact, Pagonis et al. (2020) show for a set of experimental data, that the DRCs obtained from OTOR and DSE fits are indistinguishable. Earlier studies, albeit not referring to the OTOR model, demonstrate the usefulness of the DSE function for determining high natural doses (e.g. Chapot et al., 2012; Timar-Gabor et al., 2012; Berger and Chen, 2011; Murray et al., 2007) and data displayed in Table A1 clearly show agreement of D_e values obtained from OTOR and DSE fits. Thus, the DSE function likely delivers reliable fits, with the only disadvantage being its less meaningful fit parameters and one extra parameter that adds to the number of uncertainty components.

Our study suggests that the dose range, for which the SSE offers reliable natural dose estimates, lies below $I = 0.63 I_{sat}$. From this follows that a D_e determined with a SSE fit is reliable when $D_{eSSE} < D_0$. As a consequence, the $D_e < 2D_0$ rule should be abandoned (see also King et al., 2018), because it does not take the parameter R into account which

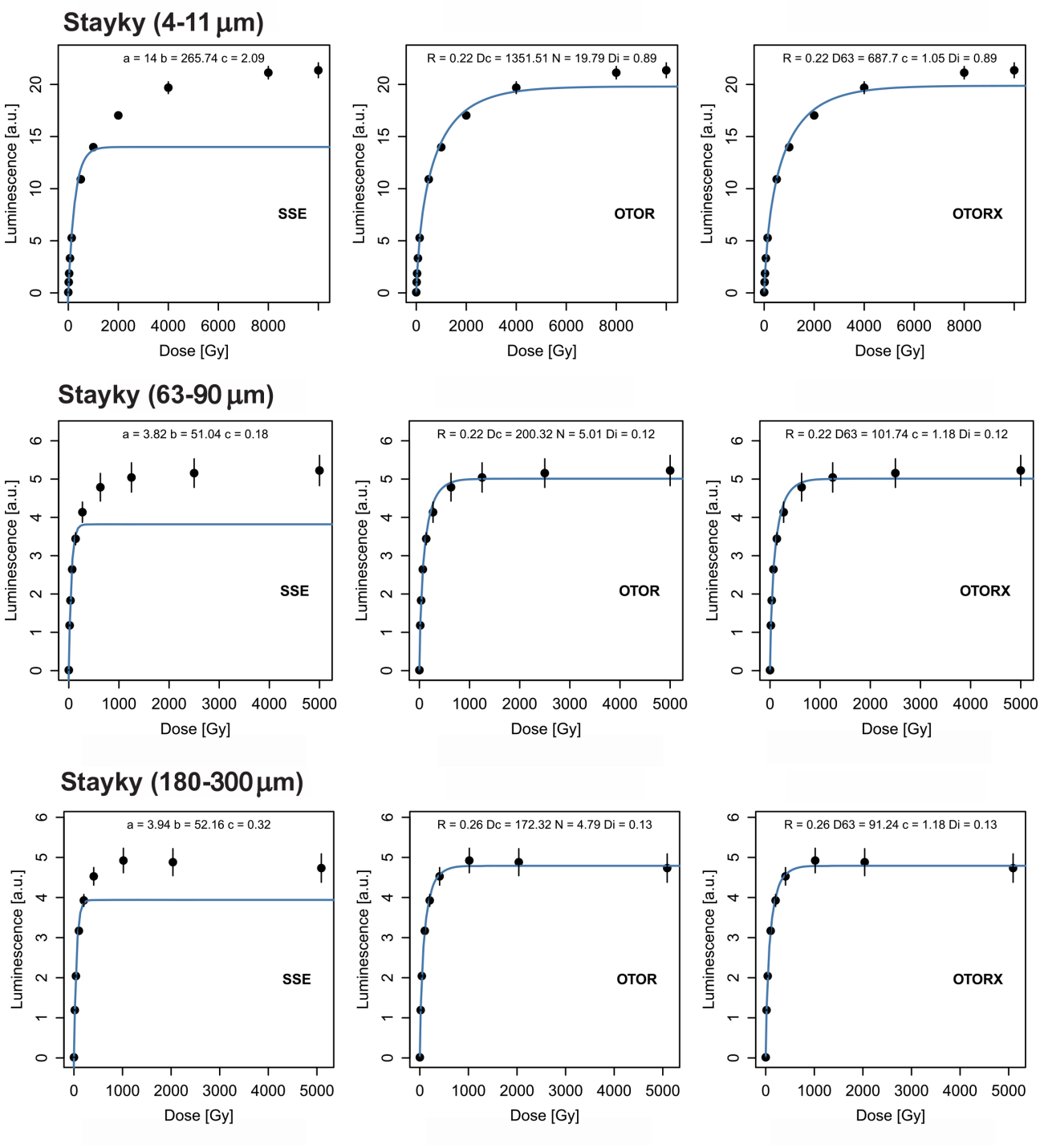

Figure 7. DRCs of small and large quartz grains (sample Stayky).

controls the shape of the DRC. Figure 9, displaying the relationship between the ratio D_{80}/D_{63} and R confirms this: For $R = 1$ the ratio is ~ 1.609 for OTOR, as it is for SSE. For $R \sim 0.26$, which is the predicted value for quartz, the ratio is ~ 1.92, hence $\sim 80\,\%$ higher than for SSE. For the calculation of these values see Appendix A.

6 Conclusions

OTOR is a phenomenological model of the simplest form with the smallest number of parameters. It is well described for a number of dosimeters including quartz. For feldspars the application is justified by the simplicity of the model

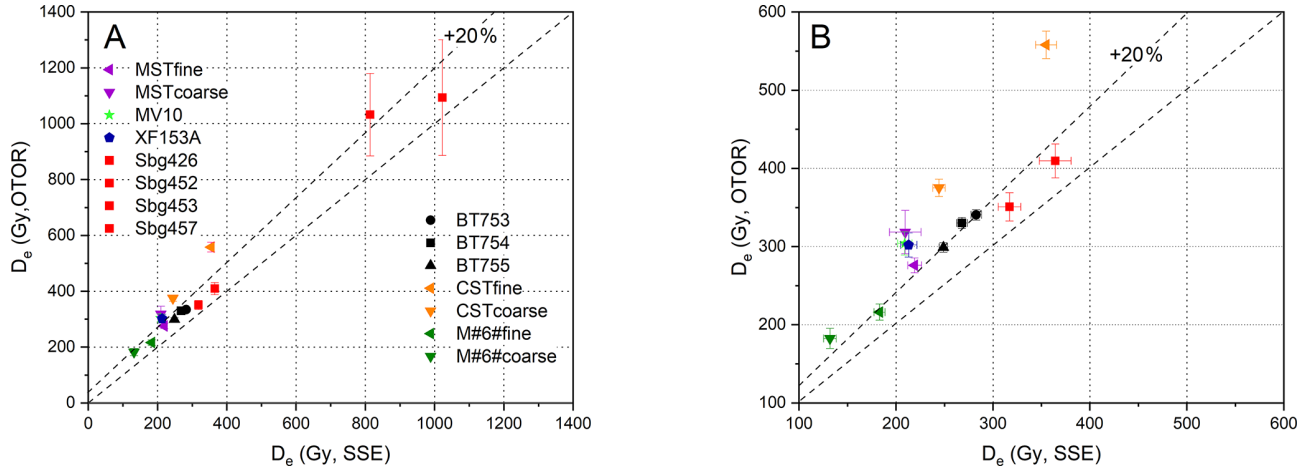

Figure 8. Comparing D_es obtained from OTOR and SSE fits. Feldspar data (red square) are not corrected for fading. **(A)** all samples analysed; **(B)** detail of **(A)** for the dose range 150–450 Gyr.

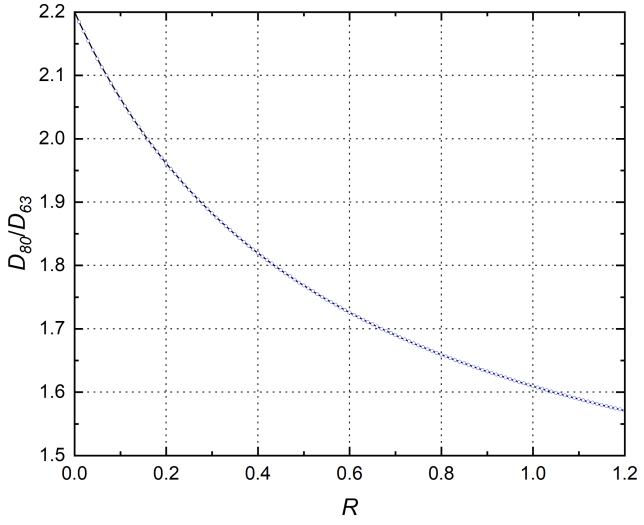

Figure 9. The ratio D_{80}/D_{63} plotted vs. R (see Eqs. A13–A15 in Appendix A for calculation).

which captures the fundamental mechanisms of irradiation and readout in many insulators. We note that R values obtained experimentally are consistent, but are generally higher for feldspars than for quartz, which confirms the pronounced sublinearity observed with most quartz DRCs.

The OTOR fit functions are most useful for multi-grain aliquot data where the luminescence intensity is the sum of light emitted by multiple grains and detected in a narrow optical window. The results from the chi-square test show much better fit quality of OTOR compared to SSE, in particular for quartz, although OTOR involves one degree of freedom more than the SSE function.

The OTOR model does not necessarily describe all dose responses possible for dosimetric materials and may well be of limited use on the single-grain level. The OTOR solutions are unable to help with complications that arise in the dosimeter due to chemical composition, crystal growth dimensions, defect locations in the crystal (e.g., Townsend et al., 2021) etc., all together making charge transfer via localised and delocalised mechanisms a complex recombination process. Moreover, using the OTOR functions to correct the DRC for fading is yet to be shown. Other functions should be taken into consideration, such as the GOK (General Order Kinetics, e.g. Guralnik et al., 2015) and the Broadly Applicable Function (Burbidge, 2015) both covering a wide range of dose responses.

Our study suggests that reliable equivalent doses are obtained from a SSE fit only when the natural dose is smaller than the characteristic saturation dose while bearing in mind that the D_0 value is always underestimated if the DRC is short and $R < 0.5$. For high natural doses, i.e. $D_e > D_0$, the SSE is unable to describe the dose response data, and this leads automatically to D_e underestimation. To avoid D_e underestimation we recommend to replace the "$2D_0$" rule with "$1D_0$" when using the SSE function for generating a DRC.

Appendix A: SSE and OTOR

In luminescence dating the single-saturating exponential function (SSE) is typically used to fit a dose response curve (DRC) to the data points obtained from a SAR protocol. The relationship between the SSE and OTOR functions is as follows: for $R = 1$, Eq. (1) in the main text reduces to:

$$F_1\left(\frac{D}{D_{63}}, 1\right) = 1 - \exp\left(\frac{-D}{D_{63}}\right) \quad \text{(A1a)}$$

where F_1 is defined by:

$$F_1\left(\frac{D}{D_{63}}, R\right) \equiv 1 + \frac{1}{(1-R)}\mathcal{W}\{-(1-R) \cdot \exp\left[-\left(1 - \frac{e-1}{e}(1-R)\right) \cdot \frac{D}{D_{63}} - (1-R)\right]\} \quad \text{(A1b)}$$

A1 OTOR and SSE for low-dose segment of the DRC

When the data obtained from a SAR measurement only cover the lower segment of a DRC composed of slope and curvature, the DRC is described by Eq. (A2) where, for reasons of simplicity, we assume no deep traps and no recuperation:

$$I = I_{\text{sat}} F_1\left(\frac{D}{D_{63}}, R-1\right) \quad \text{(A2)}$$

The low-dose segment of the DRC is short enough to be accurately described by a quadratic polynomial which allows to expand Eq. (A2) into a Taylor series for low dose:

$$I = \frac{[1+(e-1)R]I_{\text{sat}}}{eRD_{63}} D - \frac{[1+(e-1)R]^2 I_{\text{sat}}}{2e^2R^3{D_{63}}^2} D^2 + \mathcal{O}(D^3) \quad \text{(A3)}$$

The same expansion is done for the SSE by setting $R = 1$ in Eq. (A3) which yields:

$$I = \frac{I_{\text{sat}}}{D_{63}} D - \frac{I_{\text{sat}}}{2{D_{63}}^2} D^2 + \mathcal{O}(D^3) \quad \text{(A4)}$$

We note that the OTOR expansion has three parameters (I_{sat}, D_{63}, R) and the SSE has two parameters (I_{sat}, D_{63}).

By fitting the low segment of the DRC, the experimental constants c_1 and c_2 are obtained:

$$I = c_1 D - c_2 D^2 \quad \text{(A5)}$$

The next step is to match the experimentally determined correlation (Eq. A5) to the OTOR model (Eq. A3) in a way that each corresponding coefficient in the two power series match. We consider that, if two polynomials of a continuous variable (D in our case) are everywhere equal, the two polynomials must have the same coefficient. Thus:

$$c_1 = \frac{[1+(e-1)R]I_{\text{sat}}}{eRD_{63}} \quad \text{(A6)}$$

$$c_2 = \frac{[1+(e-1)R]^2 I_{\text{sat}}}{2e^2R^3D_{63}^2} \quad \text{(A7)}$$

In Eqs. (A6) and (A7), c_1 and c_2 are known from experiment, $e \sim 2.718$ is the known constant and the parameters D_{63}, R and I_{sat} are unknowns. Thus, we have two equations and three unknows. As a consequence, determining D_{63} (OTOR) from a low-dose segment of the DRC involves large error margins. Conversely, D_0 (SSE) determined from a low-dose segment of the DRC, is precise when assuming $R = 1$ (see Eq. A12 and Fig. 2 in main text for detail). To solve the problem of OTOR, we assign a predicted value to R and solve Eqs. (A6) and (A7) to obtain I_{sat} and D_{63} in terms of the experimental constants c_1 and c_2:

$$D_{63} = \frac{[1+(e-1)R]c_1}{2eR^2c_2} \quad \text{(A8)}$$

$$I_{\text{sat}} = \frac{eR}{[1+(e-1)R]} D_{63c1} = \frac{c_1^2}{2R_{c2}} \quad \text{(A9)}$$

For SSE which assumes $R = 1$, the above equations (Eqs. A8 and A9) simplify to:

$$D_{63} = \frac{c_1}{2c_2} \quad \text{(A10)}$$

$$I_{\text{sat}} = \frac{c_1^2}{2c_2} \quad \text{(A11)}$$

Next, we analyse how much error is incurred when assuming a fixed R to use for fitting. We compare, for a given c_1 and c_2, the D_{63} value (OTOR) computed at value R to the value of D_0 (SSE) computed for $R = 1$. Taking the ratio of Eq. (A8) to (A9):

$$\frac{D_{63}}{D_0} = \frac{1+(e-1)R}{eR^2} \quad \text{(A12)}$$

For the plot of Eq. (A12) see Fig. 2 in main text.

A2 D_{63} and D_{80}

D_{63} is the dose at which the OSL response is 63.2 % of its saturated value. D_{80} is the same for 80 % of the saturated value. Excluding recuperation, the formulation is:

For OTOR:

$$D_{63} = \left[\frac{1}{e} - \left(1 - \frac{1}{e}\right)R\right] D_{\text{c}} \approx (0.367 + 0.633R) D_{\text{c}} \quad \text{(A13)}$$

$$D_{80} = D_{63}\left[\frac{\ln(5) - \frac{4}{5}(1-R)}{1-(1-\frac{1}{e})(1-R)}\right] \approx D_{63}\left[\frac{0.809 + 0.800R}{0.368 + 0.632R}\right] \quad \text{(A14)}$$

For SSE:

$$I = \left(1 - \frac{1}{e}\right) I_{\text{sat}} \text{ when } D = D_0 \quad \text{(A15)}$$

$$D_{80} = D_0 \ln(5) \approx 1.609 D_0 \quad \text{(A16)}$$

For the relationship of D_0 or D_{63} to D_{80} for SSE and OTOR see Fig. 9 in main text.

Table A1. D_e values obtained for samples analysed in this study. DSE (double saturating exponential function) data with star (*) were obtained from Timar-Gabor et al. (2012). Note the differences in D_e for quartz samples with generally high natural dose which are likely the result of different fit algorithms and small number of aliquot data used.

Sample, Grain Size	Dosimeter	D_e (Gyr; SSE)	D_e (Gyr; OTOR)	D_e (Gyr; DSE)
$BT753_{4-11}$	Quartz	286 ± 5	341 ± 7	344 ± 7
$BT754_{4-11}$	Quartz	268 ± 5	330 ± 7	335 ± 7
$BT755_{4-11}$	Quartz	249 ± 4	299 ± 11	301 ± 6
$CAC_2.1_{4-11}$	Quartz	102 ± 3	112 ± 4	100 ± 4
$CAC_2.1_{63-90}$	Quartz	90 ± 2	127 ± 4	129 ± 5
CST_inf_{4-11}	Quartz	360 ± 9	558 ± 20	650 ± 20*
CST_inf_{63-90}	Quartz	246 ± 5	375 ± 9	628 ± 47*
$M\#6\#_{4-11}$	Quartz	183 ± 7	216 ± 11	206 ± 12
$M\#6\#_{63-90}$	Quartz	133 ± 7	183 ± 12	187 ± 14
$MST19_{4-11}$	Quartz	220 ± 6	276 ± 10	289 ± 9*
$MST19_{63-90}$	Quartz	210 ± 14	319 ± 37	288 ± 57*
$MV10_{4-11}$	Quartz	213 ± 8	304 ± 16	310 ± 9*
$XF_153_A_{4-11}$	Quartz	208 ± 7	293 ± 16	304 ± 23
Sbg 426_{4-11}	Feldspar	814 ± 144	1033 ± 148	1090 ± 152
Sbg 452_{4-11}	Feldspar	1022 ± 258	1094 ± 221	1075 ± 235
Sbg $453_{180-300}$	Feldspar	318 ± 13	351 ± 16	355 ± 17
Sbg $457_{180-300}$	Feldspar	365 ± 16	410 ± 24	404 ± 25

Code availability. The R script is available at Zenodo (https://doi.org/10.5281/zenodo.21226350; Mauz et al., 2026).

The Python code written for OTORX is available at https://github.com/jll2/LumDRC (Lawless and Timar-Gabor, 2024).

Data availability. Scripts used to generate the data as well as details of the data are available at Zenodo, https://doi.org/10.5281/zenodo.21226350 (Mauz et al., 2026).

Author contributions. BM developed the idea of the study based on a suggestion obtained from SK. JL supported concept and design and carried out computational work and mathematical formulation. SK carried out data analysis and generated the empirical data. All authors contributed to interpretation of results, and to text writing.

Competing interests. At least one of the (co-)authors is a member of the editorial board of *Geochronology*. The peer-review process was guided by an independent editor, and the authors also have no other competing interests to declare.

Disclaimer. Publisher's note: Copernicus Publications remains neutral with regard to jurisdictional claims made in the text, published maps, institutional affiliations, or any other geographical representation in this paper. The authors bear the ultimate responsibility for providing appropriate place names. Views expressed in the text are those of the authors and do not necessarily reflect the views of the publisher.

Acknowledgements. We thank Alida-Timar-Gabor(Babeş-Bolyai University) and her collaborators for providing numerous and highly valuable high-dose data. We thank Albert Cabré Cano (University of Erlangen) for making available aeolian feldspar samples and Michael Discher (University of Salzburg) for supporting measurements.

Financial support. This research has been supported by the Deutsche Forschungsgemeinschaft (grant no. 505822867) and the Natural Environment Research Council (grant no. NE/W00075X/1).

Review statement. This paper was edited by Sumiko Tsukamoto and reviewed by three anonymous referees.

References

Arnold, L. J., Duval, M., Demuro, M., Spooner, N. A., Santonja, M., and Pérez-González, A.: OSL dating of individual quartz 'supergrains' from the Ancient Middle Palaeolithic site of Cuesta de la Bajada, Spain, Quat. Geochronol., 36, 78–101, https://doi.org/10.1016/j.quageo.2016.07.003, 2016.

Avram, A., Constantin, D., Veres, D., Kelemen, S., Obreht, I., Hambach, U., Marković, S. B., and Timar-Gabor, A.: Testing polymineral post-IR IRSL and quartz SAR-OSL protocols on Middle to Late Pleistocene loess at Batajnica, Serbia, Boreas, 49, 615–633, https://doi.org/10.1111/bor.12442, 2020.

Avram, A., Constantin, D., Hao, Q., and Timar-Gabor, A.: Optically stimulated luminescence dating of loess in South-Eastern China using quartz and polymineral fine grains, Quat. Geochronol., 67, 101226, https://doi.org/10.1016/j.quageo.2021.101226, 2022.

Avram, A., Mason, J. A., Del Valle Villalonga, L., Constantin, D., Grecu, S., Veres, D., Marković, S., and Timar-Gabor, A.: Revisiting the chronology of a key loess section in North America using multiple luminescence dating methods, Geol. Soc. Am. B., 137, 3207–3220, https://doi.org/10.1130/B38165.1, 2025.

Bailey, R. M.: Towards a general kinetic model for optically and thermally stimulated luminescence of quartz, Radiat. Meas., 33, 17–45, https://doi.org/10.1016/S1350-4487(00)00100-1, 2001.

Bailey, R. M.: Paper I – simulation of dose absorption in quartz over geological timescales and its implications for the precision and accuracy of optical dating, Radiat. Meas., 38, 299–310, https://doi.org/10.1016/j.radmeas.2003.09.005, 2004.

Berger, G. W. and Chen, R.: Error analysis and modelling of double saturating exponential dose response curves from SAR OSL dating, ATL, 29, 9–14, https://doi.org/10.26034/la.atl.2011.444, 2011.

Bulur, E. and Özer, A. M.: Comment on: A cautionary note: apparent sensitivity change resulting from curve fitting, ATL, 10, 12–14, https://doi.org/10.26034/la.atl.1992.191, 1992.

Burbidge, C. I.: A broadly applicable function for describing luminescence dose response, J. Applied Phys., 118, 044904, https://doi.org/10.1063/1.4927214, 2015.

Chapot, M. S., Roberts, H. M., Duller, G. A. T., and Lai, Z. P.: A comparison of natural- and laboratory-generated dose response curves for quartz optically stimulated luminescence signals from Chinese Loess, Radiat. Meas., 47, 1045–1052, https://doi.org/10.1016/j.radmeas.2012.09.001, 2012.

Cunningham, A. C. and Wallinga, J.: Selection of integration time intervals for quartz OSL decay curves, Quat. Geochronol., 5, 657–666, https://doi.org/10.1016/j.quageo.2010.08.004, 2010.

Duller, G. A. T.: Improving the accuracy and precision of equivalent doses determined using the optically stimulated luminescence signal from single grains of quartz, Radiat. Meas., 47, 770–777, https://doi.org/10.1016/j.radmeas.2012.01.006, 2012.

Fuchs, M., Kreutzer, S., Rousseau, D. D., Antoine, P., Hatté, C., Lagroix, F., Moine, O., Gauthier, C., Svoboda, J., and Lisá, L.: The loess sequence of Dolní Věstonice, Czech Republic: A new OSL-based chronology of the last climatic cycle, Boreas, 42, 664–677, https://doi.org/10.1111/j.1502-3885.2012.00299.x, 2013.

Fuchs, M., Kreutzer, S., Rousseau, D.-D., Antoine, P., Hatté, C., Lagroix, F., Moine, O., Gauthier, C., Svoboda, J., and Lisá, L.: The loess sequence of Dolní Věstonice, Czech Republic: A new OSL-based chronology of the last climatic cycle, Zenodo [data set], https://doi.org/10.5281/zenodo.8246533, 2023.

Grün, R. and Rhodes, E. J.: Simulations of saturating exponential ESR/TL dose response curves – weighting of intensity values by inverse variance, ATL, 10, 50–56, https://doi.org/10.26034/la.atl.1992.202, 1992.

Guralnik, B. and King, G. E.: Anomalous fading correction in luminescence dating – a mathematical reappraisal, Geochronology, 8, 589–606, https://doi.org/10.5194/gchron-8-589-2026, 2026.

Guralnik, B., Li, B., Jain, M., Chen, R., Paris, R. B., Murray, A. S., Li, S.-H., Pagonis, V., Valla, P. G., and Herman, F.: Radiation-induced growth and isothermal decay of infrared-stimulated luminescence from feldspar, Radiat. Meas., 81, 224–231, https://doi.org/10.1016/j.radmeas.2015.02.011, 2015.

Hayes, R. B., Haskell, E. H., and Kenner, G. H.: An assessment of the Levenberg-Marquardt fitting algorithm on saturating exponential data sets, Ancient TL, 16, 57–62, https://doi.org/10.26034/la.atl.1998.294, 1998.

Hu, Y., Li, B., and Jacobs, Z.: Single-Grain Quartz OSL Characteristics: Testing for Correlations within and between Sites in Asia, Europe and Africa, MPs, 3, 2, https://doi.org/10.3390/mps3010002, 2019.

Huntley, D. J., Short, M. A., and Dunphy, K.: Deep traps in quartz and their use for optical dating, Can. J. Phys., 74, 81–91, 1996.

Kars, R. H., Wallinga, J., and Cohen, K. M.: A new approach towards anomalous fading correction for feldspar IRSL dating – tests on samples in field saturation, Radiat. Meas., 43, 786–790, https://doi.org/10.1016/j.radmeas.2008.01.021, 2008.

King, G. E., Burow, C., Roberts, H. M., and Pearce, N. J. G.: Age determination using feldspar: Evaluating fading-correction model performance, Radiat. Meas., 119, 58–73, https://doi.org/10.1016/j.radmeas.2018.07.013, 2018.

Kitis, G., Polymeris, G. S., and Pagonis, V.: Stimulated luminescence emission: From phenomenological models to master analytical equations, Appl. Radiat. Isotopes, 153, 108797, https://doi.org/10.1016/j.apradiso.2019.05.041, 2019.

Kitis, G., Peng, J., Li, B., and Pagonis, V.: Testing new analytical expression for dose response curves originating from the OTOR model, J. Lumin., 244, 118747, https://doi.org/10.1016/j.jlumin.2022.118747, 2022.

Kitis, G., Polymeris, G. S., and Peng, J.: Determining equivalent dose for optically stimulated luminescence (OSL) dating with physically meaningful dose response curves, Quat. Geochronol., 88, 101671, https://doi.org/10.1016/j.quageo.2025.101671, 2025.

Kreutzer, S., Burow, C., Dietze, M., Fuchs, M. C., Schmidt, C., Fischer, M., Friedrich, J., Mercier, N., Philippe, A., Riedesel, S., Autzen, M., Mittelstrass, D., Gray, H. J., Galharret, J.-M., Colombo, M., Steinbuch, L., de Boer, A.-M., and Bluszcz, A.: Luminescence: Comprehensive luminescence dating data analysis (1.2.1), CRAN [code], https://doi.org/10.32614/CRAN.package.Luminescence, 2026.

Lawless, J. L. and Timar-Gabor, A.: A new analytical model to fit both fine and coarse grained quartz luminescence dose response curves, Radiat. Meas., 170, 107045, https://doi.org/10.1016/j.radmeas.2023.107045, 2024 (code available at: https://github.com/jll2/LumDRC, last access: May 2026).

Lawless, J. L., Chen, R., Lo, D., and Pagonis, V.: A model for non-monotonic dose dependence of thermoluminescence (TL), J. Phys.: Condens. Matter, 17, 737–753, https://doi.org/10.1088/0953-8984/17/4/016, 2005.

Lawless, J. L., Chen, R., and Pagonis, V.: Sublinear dose dependence of thermoluminescence and optically stimulated luminescence prior to the approach to saturation level, Radiat. Meas., 44, 606–610, https://doi.org/10.1016/j.radmeas.2009.03.003, 2009.

Li, B., Jacobs, Z., and Roberts, R. G.: Investigation of the applicability of standardised growth curves for OSL dating of quartz from Haua Fteah cave, Libya, Quat. Geochronol., 35, 1–15, https://doi.org/10.1016/j.quageo.2016.05.001, 2016.

Lowick, S. E. and Preusser, F.: Investigating age underestimation in the high dose region of optically stimulated luminescence using fine grain quartz, Quat. Geochronol., 6, 33–41, https://doi.org/10.1016/j.quageo.2010.08.001, 2011.

Lyons, R. G., Brennan, B. J., Hosking, P. L., and Brennan, B. J.: Estimation of accumulated dose and its uncertainties: potential pitfalls in curve fitting, ATL, 10, 42–49, https://doi.org/10.26034/la.atl.1992.201, 1992.

Mauz, B., Kreutzer, S., and Lawless, J.: Improving the estimation of high natural luminescence doses using OTOR solutions for SAR-derived data (Version 1.0), Zenodo [data set], https://doi.org/10.5281/zenodo.21226350, 2026.

Moré, J. J., Garbow, B. S., and Hillstrom, K. E.: User Guide for MINPACK-1, https://cds.cern.ch/record/126569/files/CM-P00068642.pdf (last access: 23 May 2026), 1980.

McKeever, W. S. and Chen, R.: Luminescence models, Radiat. Meas. 27, 625–661, https://doi.org/10.1016/S1350-4487(97)00203-5, 1997.

Meszner, S., Kreutzer, S., Fuchs, M., and Faust, D.: Late Pleistocene landscape dynamics in Saxony, Germany: Paleoenvironmental reconstruction using loess-paleosol sequences, Quaternary Int., 296, 94–107, https://doi.org/10.1016/j.quaint.2012.12.040, 2013.

Moska, P., Adamiec, G., and Jary, Z.: High resolution dating of loess profile from Biały Kościół, south–west Poland, Quat. Geochronol., 10, 87–93, https://doi.org/10.1016/j.quageo.2012.04.003, 2012.

Murray, A. S. and Wintle, A. G.: The single aliquot regenerative dose protocol: potential for improvements in reliability, Radiat. Meas., 37, 377–381, https://doi.org/10.1016/S1350-4487(03)00053-2, 2003.

Murray, A. S., Svendsen, J. I., Mangerud, J., and Astakhov, V. I.: Testing the accuracy of quartz OSL dating using a known-age Eemian site on the river Sula, northern Russia, Quat. Geochronol., 2, 102–109, https://doi.org/10.1016/j.quageo.2006.04.004, 2007.

Murray, A., Arnold, L. J., Buylaert, J.-P., Guerin, G., Qin, J., Singhvi, A. S., Smedley, R. and Thomsen, K. J.: Optically stimulated luminescence dating using quartz. Nature Reviews, Methods Primers, 1, 72, https://doi.org/10.1038/s43586-021-00068-5, 2021.

Pagonis, V., Kitis, G., and Chen, R.: A new analytical equation for the dose response of dosimetric materials, based on the Lambert W function, J. Lumin., 225, 117333, https://doi.org/10.1016/j.jlumin.2020.117333, 2020.

Peng, J. and Li, B.: Single-aliquot Regenerative-Dose (SAR) and Standardised Growth Curve (SGC) Equivalent Dose Determination in a Batch Model Using the R Package 'numOSL', Ancient TL, 35, 32–53, https://doi.org/10.26034/la.atl.2017.516, 2017.

Peng, J., Wang, X., and Adamiec, G.: The build-up of the laboratory-generated dose-response curve and underestimation of equivalent dose for quartz OSL in the high dose region: A critical modelling study, Quat. Geochronol., 67, 101231, https://doi.org/10.1016/j.quageo.2021.101231, 2022.

R Core Team: R: A language and environment for statistical computing (v4.6.0), https://r-project.org/ (last access: 23 May 2026), 2026.

Singarayer, J. S. and Bailey, R. M.: Component-resolved bleaching spectra of quartz optically stimulated luminescence: preliminary results and implications for dating, Radiat. Meas., 38, 111–118, https://doi.org/10.1016/S1350-4487(03)00250-6, 2004.

Thomsen, K. J., Murray, A. S., Jain, M., and Bøtter-Jensen, L.: Laboratory fading rates of various luminescence signals from feldspar-rich sediment extracts, Radiat. Meas., 43, 1474–1486, https://doi.org/10.1016/j.radmeas.2008.06.002, 2008.

Thomsen, K. J., Murray, A. S., Buylaert, J. P., Jain, M., Hansen, J. H., and Aubry, T.: Testing single-grain quartz OSL methods using sediment samples with independent age control from the Bordes-Fitte rockshelter (Roches d'Abilly site, Central France), Quat. Geochronol., 31, 77–96, https://doi.org/10.1016/j.quageo.2015.11.002, 2016.

Timar, A., Vandenberghe, D., Panaiotu, E. C., Panaiotu, C. G., Necula, C., Cosma, C., and Van Den Haute, P.: Optical dating of Romanian loess using fine-grained quartz, Quat. Geochronol., 5, 143–148, https://doi.org/10.1016/j.quageo.2009.03.003, 2010.

Timar-Gabor, A., Vasiliniuc, Ş., Vandenberghe, D. A. G., Cosma, C., and Wintle, A. G.: Investigations into the reliability of SAR-OSL equivalent doses obtained for quartz samples displaying dose response curves with more than one component, Radiat. Meas., 47, 740–745, https://doi.org/10.1016/j.radmeas.2011.12.001, 2012.

Timar-Gabor, A. and Wintle, A. G.: On natural and laboratory generated dose response curves for quartz of different grain sizes from Romanian loess, Quat. Geochronol., 18, 34–40, https://doi.org/10.1016/j.quageo.2013.08.001, 2013.

Timar-Gabor, A., Constantin, D., Buylaert, J. P., Jain, M., Murray, A. S., and Wintle, A. G.: Fundamental investigations of natural and laboratory generated SAR dose response curves for quartz OSL in the high dose range, Radiat. Meas., 81, 150–156, https://doi.org/10.1016/j.radmeas.2015.01.013, 2015.

Timar-Gabor, A., Buylaert, J.-P., Guralnik, B., Trandafir-Antohi, O., Constantin, D., Anechitei-Deacu, V., Jain, M., Murray, A. S., Porat, N., Hao, Q., and Wintle, A. G.: On the importance of grain size in luminescence dating using quartz, Radiat. Meas., 106, 464–471, https://doi.org/10.1016/j.radmeas.2017.01.009, 2017.

Townsend, P. D., Wang, Y., and McKeever, S. W. S.: Spectral evidence for defect clustering: Relevance to radiation dosimetry materials, Radiat. Meas., 147, 106634, https://doi.org/10.1016/j.radmeas.2021.106634, 2021.

Tribolo, C., Mercier, N., Dumottay, C., Cantin, N., Banks, W. E., Stratford, D., De La Peña, P., Backwell, L., Wadley, L., and d'Errico, F.: Luminescence dating at Border Cave: attempts, questions, and new results, Quaternary Sci. Rev., 296, 107787, https://doi.org/10.1016/j.quascirev.2022.107787, 2022.

Veres, D., Tecsa, V., Gerasimenko, N., Zeeden, C., Hambach, U., and Timar-Gabor, A.: Short-term soil formation events in last glacial east European loess, evidence from multimethod luminescence dating, Quaternary Sci. Rev., 200, 34–51, https://doi.org/10.1016/j.quascirev.2018.09.037, 2018.

Wintle, A. G. and Murray, A. S.: A review of quartz optically stimulated luminescence characteristics and their relevance in single-aliquot regeneration dating protocols, Radiat. Meas., 41, 369–391, https://doi.org/10.1016/j.radmeas.2005.11.001, 2006.

Yoshida, H., Roberts, R. G., Olley, J. M., Laslett, G. M., and Galbraith, R. F.: Extending the age range of optical dating using single 'supergrains' of quartz, Radiat. Meas., 32, 439–446, https://doi.org/10.1016/S1350-4487(99)00287-5, 2000.